Journal of Petroleum Exploration and Production Technology (2024) 14:535–553
https://doi.org/10.1007/s13202-023-01716-0

ORIGINAL PAPER-PRODUCTION ENGINEERING

Treatment of paraffin deposition behavior in gas-condensate wells with chemical inhibitors

Bowen Shi[1] · Jiajun Hong[1] · Zhihua Wang[1] · Zhenbo Chang[1] · Feng Li[2]

Received: 3 March 2023 / Accepted: 13 October 2023 / Published online: 2 November 2023

Abstract

As deep gas-condensate reservoirs are explored, the problem of paraffin deposition is becoming more prominent. Therefore, this paper collects condensate samples from representative paraffin deposition gas-condensate wells and analyzes basic physical properties. The cold plate deposition device is employed to study paraffin deposition behavior under well conditions and to divide the critical regions for paraffin deposition in gas-condensate wells. The experimental apparatus, such as the crude oil dynamic paraffin deposition rate tester, is utilized to investigate the preventive effect of paraffin dispersants and paraffin crystal modifier. The results show that there is significant phase change behavior in gas-condensate wells and gas phase is dominant form, but there is also phase evolution. It can be identified from the experiments that paraffin deposition is mainly located in the 1000 ~ 1500 m region, and a paraffin deposition identification chart has been established. The maximum deposition rate could reach 15.50 mm/year, which matched the temperature and pressure conditions of 45 ℃ and 70 MPa. The preventive effect of paraffin crystal modifiers greatly exceeds that of paraffin dispersants, with paraffin prevention rates of 85–95% at the optimal concentrations of 0.25–0.50 wt.%. The dissolving paraffin rate can reach 0.0169 g/min. It decreases the paraffin appearance temperature approximately 40% and significantly changes the paraffin crystal morphology. Increased deposition surface area of the cold plate structural design describes the paraffin deposition. This diagram facilitates the reliable identification of paraffin deposition areas and the deposition rates in the wellbore during production. The optimum amounts of BZ and PI paraffin inhibitors are quantified. This study provides a comprehensive understanding of the paraffin deposition behavior, and scientific basis and guidance for the selection of paraffin inhibitors in gas-condensate wells.

Keywords Paraffin deposition · Paraffin crystal modifier · Phase behavior · Deposition rate · Gas-condensate wells

List of symbols

a	The parameter
b	The parameter
CM	The crystal modifier
DSC	The differential scanning calorimetry
$\exp\left(\int_{P_0}^{P}\frac{V_i^S}{RT}\mathrm{d}P\right)$	The effect of pressure on solid phase
$\exp\left(\int_{P_0}^{P}\frac{V_i^L}{RT}\mathrm{d}P\right)$	The effect of pressure on liquid phase
$f_i^S\left(T,P,x^S\right)$	The fugacity of component i in the solid phase and is the same as f_i^S
$f_i^L\left(T,P,x^L\right)$	The fugacity of component i in the liquid phase and is the same as f_i^L
K_i^{SL}	The solid–liquid phase equilibrium constant of the component i
K_i^{VL}	The gas–liquid equilibrium constant of the component i
L	The liquid phase molar fraction, (L/mol)
P	The system pressure, (Pa)
P_0	The atmospheric pressure 0.101325 MPa
P_c	The critical pressure, (Pa)
PPD	The pour-point depressant
R	The ideal gas constant, (kJ/(kmol·K))
S	The molar fraction of solid phase
T	The system temperature, (K)
T_r	The ratio of absolute to critical temperature, (K)

✉ Zhihua Wang
zhihua_wang@nepu.edu.cn; zhihua_wang@126.com

[1] Key Laboratory for Enhanced Oil & Gas Recovery of the Ministry of Education, Northeast Petroleum University, Daqing 163318, China

[2] Gree Energy Services, Inc., Shenzhen 518100, Guangdong, China

T_c	The critical temperature, (K)
V	The molar volume of the gas or liquid phase
WAT	The wax appearance temperature
x_i^S	The molar fraction of component i in the solid phase
x_i^L	The molar fraction of component i in the liquid phase
z_i	The molar composition of component i
$\alpha(T)$	The temperature correlation for pure materials
γ_i^S	The activity coefficient of component i in solid phase
γ_i^L	The activity coefficient of component i in liquid phase
ω	The acentric factor

Introduction

Gas-condensate reservoir is a special kind of reservoirs with large depth, high pressure, and high temperature, which is mainly distributed in Russia, the Middle East, Central Asia, and the United States (Behesht et al. 2021; Han et al. 2021; Zhong et al. 2022). When the pressure in the wellbore is lower than saturation pressure, a retrograde condensation phenomenon will be occurred in the region, resulting in unnecessary energy and productivity losses (Ghiasi et al. 2014; Faraji et al. 2020; Wang et al. 2022a, b, c, d). However, gas-condensate reservoirs are still facing from moderate to severe paraffin deposition problems during the extraction process, and even experiencing wellbore blockages due to their phase change and precipitation properties (Shi et al. 2022; Sousa et al. 2019; Ragunathan et al. 2022a).

The mechanism of paraffin deposition

As pressure and temperature conditions in gas-condensate wells change, heavy components such as paraffin, resin, and asphaltene will easily precipitate as solids and lead to paraffin deposition on the wellbore (Lekomtsev et al. 2022). Paraffin deposition makes the effective flow area of the wellbore reduced, increases the flow resistance, reduces the transportation capacity and even blocks the wellbore under severe conditions (Danilović et al. 2010; Ragunathan et al. 2022b). There are four main mechanisms of paraffin deposition, such as molecular diffusion, shear dispersion, Brownian diffusion, and shear stripping (Wang et al. 2020). Scholars generally think the molecular diffusion as the dominant mechanism of paraffin deposition (Singh et al. 2000; Huang et al. 2011). The molecular diffusion mechanism shows that when the wellbore temperature is lower than temperature of condensate and paraffin appearance, paraffin molecules will crystallize and precipitate at the inner wall of the wellbore and mechanical impurities (Van der Geest et al. 2021; Gan et al. 2019). Therefore, it will form radial concentration gradient of paraffin molecules between oil flow and the rough wall (Sousa et al. 2020; Wang et al. 2022a; Xu et al. 2021). When a velocity gradient exists in the wellbore, the oil flow is faster in the center than the walls, there will be a potential risk of paraffin deposition. Under the shearing action, the paraffin crystals, resins and asphaltenes suspended in the oil flow will move in a rotational motion at a certain angular velocity, resulting in the paraffin crystals, resins and asphaltenes to migrate from the center of the oil flow toward the wall, and occur paraffin deposition behavior (Wang et al. 2019; Ochieng et al. 2022). Brownian motion is the irregular movement of paraffin crystals suspended in the oil flow under high-temperature conditions. This continuously random process increases the chances of the paraffin crystals colliding, agglomerating and cross-linking into large particles to further agglomerate into the nucleus (Hong et al. 2023). Under the radial concentration gradient, paraffin crystals move from high concentration areas to low concentration areas, migrate toward the wall, and form paraffin depositions on the wall (Azevedo and Teixeira 2003; Wang et al. 2022b). Paraffin deposition rates increase with increasing flow velocity at low flow rates and decrease with increasing flow velocity under higher flow conditions. In the turbulent phase, the shear stripping effect becomes dominant (Wang et al. 2022c). The higher the flow rate is, the higher dispersion rate of the paraffin molecules is, and the stronger molecular diffusion is, even and the shear stripping effect is also increased (Hernandez et al. 2004; Zhao et al. 2022).

Van Der Geest et al. (2018) employed the DSC and CEPETRO experiment apparatus to determine molecular diffusion as a mechanism for paraffin deposition by investigating Brazilian crude oil. Mahir et al. (2019) proved that concentration gradient and temperature gradient are the key factors contributing to paraffin deposition and deposition layer aging by the cold finger apparatus. Chi et al. (2017) identified the temperature gradient as a key element in the promotion of paraffin deposition by the cold finger and flow loop experiments considering both with and without paraffin inhibitor dosing conditions. Szuflita et al. (2020) studied the effect of three paraffin inhibitors on paraffin deposition by the PVT experiment apparatus to clarify the prediction curve of paraffin deposition with temperature decrease. Hoffmann and Amundsen (2009) utilized deposition flow loop experiments to study waxy condensate in the North Sea, analyzed the deposition

thickness by laser techniques, and confirmed molecular diffusion as the key mechanism for the paraffin deposition.

The mechanism of paraffin inhibitors

Chemical paraffin inhibitors are agents that could slow down or prevent the precipitation, growth, aggregation or deposition of paraffin crystals on solid surfaces (Elganidi et al. 2022; Wang et al. 2023). Chemical paraffin prevention has three methods which are paraffin dispersants, paraffin inhibitor (paraffin crystal modifier) and pour-point depressant (PPD) (Anisuzzaman et al. 2017; Ragunathan et al. 2020). Scholars have summarized four points on the mechanisms of chemical paraffin inhibitors by long-term research on chemical paraffin prevention (Makwashi et al. 2021). Co-crystallization theory indicates that the paraffin inhibitor crystallizes together with the paraffin component at the paraffin appearance temperature. The inhibitor molecule has the same structure as the paraffin molecule and can be combined with the paraffin component to form co-crystallization phenomenon. The inhibitor molecule also has a part of different structures to the paraffin molecule, which prevents the further growth of paraffin crystals (Zhang et al. 2003). The nucleation theory is also called paraffin crystallization center theory. Due to the melting point of inhibitors is higher than paraffin appearance temperature, therefore, as the oil temperature decreases, the inhibitors will crystallize before the paraffin components. They become the nucleation center of paraffin crystals, which makes an increase in the number of tiny paraffin crystals compared to that without the addition, and it is not easy to form larger paraffin crystals (Ibrahim et al. 2023). The solubilization theory indicates that adding inhibitors could increase the solubility of paraffin, decrease the amount of paraffin precipitated, and improve the dispersion of paraffin. The crystallization theory also indicates that injecting inhibitors improves the solubility of the solute, which decreases the supersaturation of the solution, therefore, reducing the paraffin growth rate and impeding the growth of paraffin crystals (Elarbe et al. 2022; Elkatory et al. 2023). The adsorption theory shows that inhibitors appear under the paraffin appearance temperature and adsorb on the surface of the paraffin crystals. This changes the original surface properties of paraffin crystals and the growth habit of the crystals. Eventually, they prevent the growth of the crystals, weaken the adhesion between the crystals, and make not form larger crystals (Ma et al. 2017; Kurniawan et al. 2021).

Objectives of the study

The present research on the paraffin deposition mechanism in this field is still mainly from experimental methods, and the description of deep high-temperature and high-pressure gas-condensate reservoirs is still relatively poor, and the research on the paraffin deposition critical boundary of gas-condensate wells and the growth rate of paraffin deposition is even more rare. The research on chemical paraffin inhibitors, likewise, has been focused on a specific agent in conventional wells, such as ethylene vinyl acetate or maleic anhydride, mainly evaluating their mechanisms and effects, but not giving precise advice on which type is more suitable for gas-condensate wells and what is the optimal amount of their effects.

In this study, we focused on understanding the treatment on paraffin deposition behavior in gas-condensate wells with chemical inhibitors. Therefore, we collected condensate samples from typical paraffin deposition gas-condensate wells in the Tarim Oilfield (China) and studied the paraffin deposition behavior of gas-condensate wells by a cold plate device. The phase behavior and phase change characteristics of condensate samples are determined by the calculated model. The temperature and pressure distributions of the gas-condensate wells gained by the actual tests were taken to modify the calculated results of the temperature and pressure profiles, and to determine the temperature and pressure profiles for different wellhead conditions. Two representative types of chemical inhibitors, such as paraffin dispersants and paraffin inhibitors (paraffin crystal modifier), were selected to further study and analyze the effect on different types of chemical inhibitors on the paraffin deposition behavior of gas-condensate wells. A comparative analysis was used to determine the more appropriate chemical inhibitor for gas-condensate wells and the mechanism. Therefore, this work fills in the critical boundary prediction of paraffin deposition in gas-condensate wells, the characterization of deposition thickness growth rate, and the optimal effective concentration of chemical paraffin inhibitors, which facilitates the prediction and treatment of paraffin deposition in the domain of gas-condensate reservoirs in future research. Hence, a guide and basis for paraffin prevention operations in gas-condensate wells was provided.

Experiments

Materials

The typical condensate samples for experiments were collected from paraffin deposition gas-condensate wells in one block of the Tarim Oilfield (China). The oil samples collected from typical wells were taken from condensate samples processed in the secondary separator, and taken in dry, clean plastic buckets to be brought back to the laboratory. The collected condensate samples were divided

Table 1 The sampling conditions for condensate samples

Sample numbers	Sampling location	Wellhead temperature, ℃	Wellhead pressure, MPa
1#	Secondary separator	21.50	86.00
2#	Secondary separator	30.20	81.89
3#	Secondary separator	52.80	55.12

into three groups based on typical wellhead conditions in the block, which were 20 ~ 30, 30 ~ 40, and 40 ~ 50 ℃. They are named 1#, 2# and 3#, as shown in Table 1. The condensate samples were classified under different wellhead static conditions to determine the paraffin deposition behavior of different well types and to provide a basis for subsequent research proposals. The condensate samples for experiments should be preheated, sheared and stirred in advance to eliminate operational history and ensure greater accuracy (Hassan et al. 2019).

We designed and constructed a high-temperature and high-pressure cold plate experiment device to investigate the paraffin deposition behavior of gas-condensate wells, and to identify deposition critical boundary (Yaghy et al. 2021; Subramanie et al. 2021). As shown in Fig. 1, the device is mainly consisted of an ultra-high pressure electric pump, an ultra-high pressure kettle body, a high-pressure reflector, a paraffin deposition plate, temperature and pressure control valves, and other components. The bearing pressure of the system is 150 MPa, the stirring speed is 0 ~ 2500 r/min, and the heat endurance of the system is −20 ~ 200 ℃.

1-High-temperature and high-pressure paraffin kettle body; 2-Paraffin deposition plate; 3-High temperature oil bath; 4-Stirring motor; 5-Stirring magnet; 6-Stirring paddle; 7-Temperature sensor; 8-Pressure sensor; 9-Visual window; 10-Constant pressure and constant speed pump; 11-Gas-condensate container; 12-Condensate container; 13-Waste liquid receiving tank; 14-Data acquisition and control system; 15-Insulation sleeve; 16-Kettle body cover; 17-Stirring seal head; 18-Kettle body medium flow control valve; 19-Discharge valve; 20-Intake control valve; 21-Intake control valve; 22-Gas volume flowmeter; 23-Liquid mass flowmeter; 24-Oil bath inlet; 25-Oil bath outlet; 26. Exhaust valve; 27-Safety valve; 28-Metal seal ring; 29-High-temperature resistant fluorrubber gasket; 30-Motor bracket; 31-Motor shaft; 32-Embedded platform; 33-Fixed plate; 34-Fixed bolt; 35-Spring buckle.

Two representative types of chemical inhibitors are selected, such as paraffin dispersants and paraffin inhibitors. These experiment apparatuses include crude oil dynamic paraffin deposition rate tester, reciprocating oscillator, differential scanning calorimeter, polarizing microscope, and microscopic imaging real-time online analysis system. Auxiliary materials are anhydrous ethanol, xylene, petroleum ether, sectioned paraffin, slides, coverslips, lens paper, etc. Some of the experiment devices are shown in Fig. 2.

Procedures

According to the general area of the field operation blocked, the temperature, pressure and temperature difference of the paraffin deposition experiment are determined and regulated by the combination of the temperature and pressure distribution of gas-condensate wells. For the condensate samples from three gas-condensate wells, the temperature and pressure ranges for the experiments were determined based on the wellhead conditions. A single modulation of temperature or pressure was employed to find the critical boundary of paraffin deposition. Then combine the temperature and pressure distributions to determine the deposition behavior and the amount of deposition under different well depth conditions. After the experiments, the deposited cold plates were weighed to determine the deposition rate and predict the critical deposition boundaries by making weight changes before and after the cold plates. The drawing process of the paraffin deposition identification chart is shown in Fig. 3.

To determine the appropriate chemical inhibitors for gas-condensate wells with paraffin deposition, we initially started with an investigation process to compare and select several proper agents. This was followed by the use of a variety of experiment devices to select the optimal type of paraffin inhibitor according to prevention effect, dosage, safety, and paraffin crystal distribution, and to analyze its actual mechanism. The detailed experimental procedure is shown in Fig. 4.

To collect paraffin inhibitors commonly used in the oilfield by many types and multiple sources, it is also necessary to initially select applicable paraffin inhibitors, considering the production conditions and the physical properties. Then, selecting superior paraffin inhibitor considering the paraffin prevention performance, paraffin dissolving performance, depressive effect, and accessibility. Finally, two optimal types of paraffin inhibitors were selected incorporating the type, mechanism, performance and dosage of paraffin inhibitors as the experimental objects.

The two types of paraffin inhibitors screened in the paper were paraffin dispersants and paraffin crystal modifiers. The BZ paraffin inhibitor is a paraffin crystal modifier, and its main component is octadecyl methacrylate, compounded with polyethylene and alkyl petroleum sulfonate, as in Fig. 5a. It is light yellow in color and oil soluble. The PI paraffin inhibitor is a paraffin dispersant, and its main component is sodium

(a) Paraffin deposition simulation experiment platform

(b) Paraffin deposition cold plates

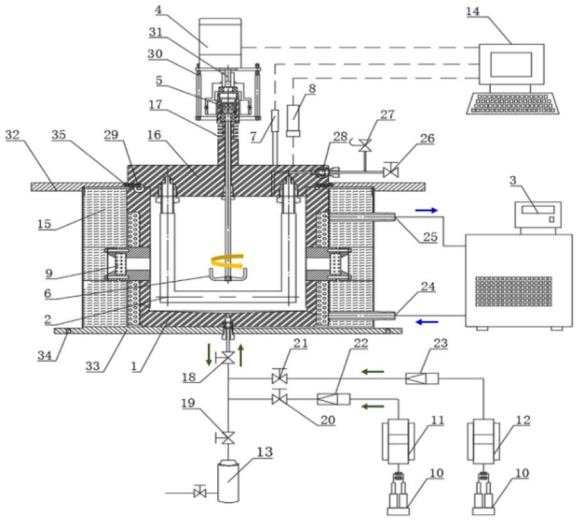

(c) The schematic diagram of the cold plate deposition device

1-High temperature and high pressure paraffin kettle body; 2-Paraffin deposition plate; 3-High temperature oil bath; 4-Stirring motor; 5-Stirring magnet; 6-Stirring paddle; 7-Temperature sensor; 8-Pressure sensor; 9-Visual window; 10-Constant pressure and constant speed pump; 11- Gas condensate container; 12-Condensate container; 13-Waste liquid receiving tank; 14-Data acquisition and control system; 15-Insulation sleeve; 16-Kettle body cover; 17-Stirring seal head; 18-Kettle body medium flow control valve; 19-Discharge valve; 20-Intake control valve; 21-Intake control valve; 22-Gas volume flowmeter; 23-Liquid mass flowmeter; 24-Oil bath inlet; 25-Oil bath outlet; 26. Exhaust valve; 27-Safety valve; 28-Metal seal ring; 29-High temperature resistant fluorrubber gasket; 30-Motor bracket; 31-Motor shaft; 32-Embedded platform; 33-Fixed plate; 34-Fixed bolt; 35-Spring buckle.

Fig. 1 Paraffin deposition experiment device

dodecylbenzene sulfonate, and compounded with polyamide and ketone, as in Fig. 5b. And it is an oil-soluble milky white liquid. Alkyl petroleum sulfonates and polyethylene can be combined to form a composite material which has the surface activity of the petroleum sulfonate and the physical properties of the polyethylene. The structural formula of the composite can be expressed as $[R\text{-}SO_3^{-M+}\text{-}CH_2\text{-}CH_2^{-}]_n$, where R denotes an alkyl chain, M denotes an alkali metal or ammonium cation, and *n* denotes the number of repeats of the polyethylene.

(a) Crude oil dynamic paraffin deposition rate tester (b) Reciprocating oscillator

Fig. 2 Paraffin inhibitor performance test device

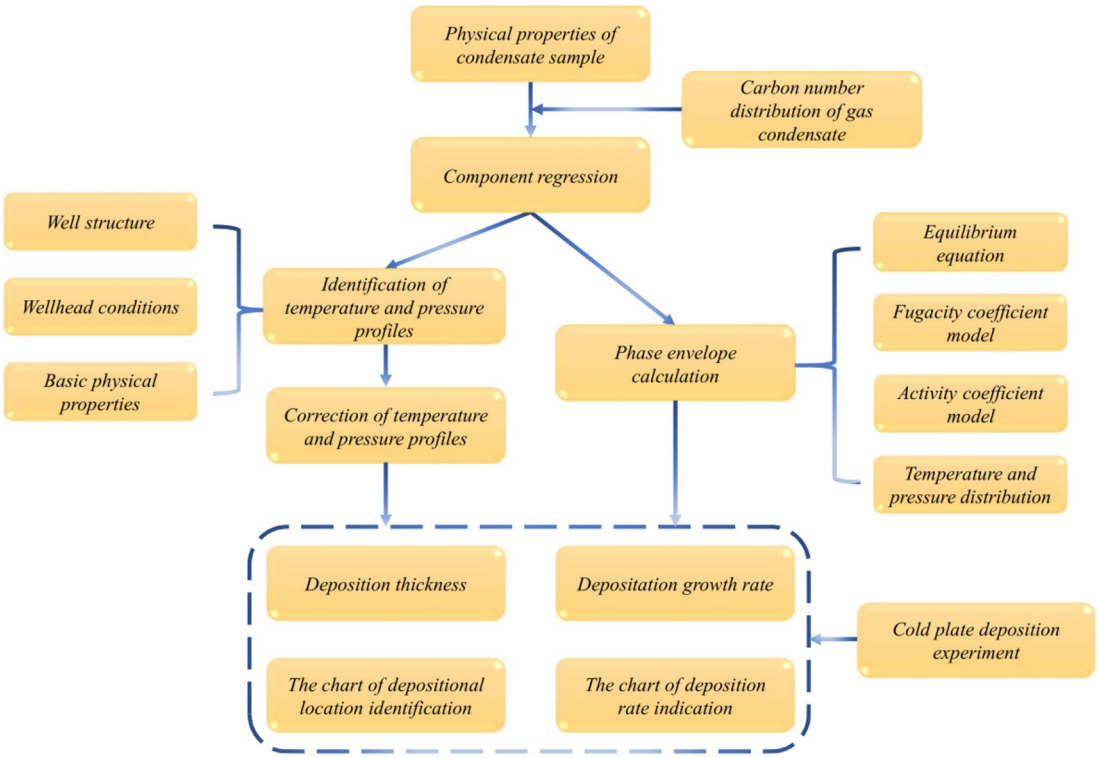

Fig. 3 The drawing process of the paraffin deposition identification chart

Mathematical method

Temperature–pressure profile

The temperature and pressure gradient interpretation data from different wells are further analyzed and used as the basis to determine the temperature–pressure profiles of gas-condensate wells and to fit to the actual conditions. The temperature and pressure distributions along the vertical depth of the wellbore are all ordered data points. Therefore, the linear fitting algorithm is employed to construct a straight-line or curve. If all parameter points are on the line, the temperature and pressure distribution is not in a mismatch status. If not, the distribution is in a mismatch status. So, the linear fitting algorithm is employed to fit the parameters to determine the temperature–pressure profile.

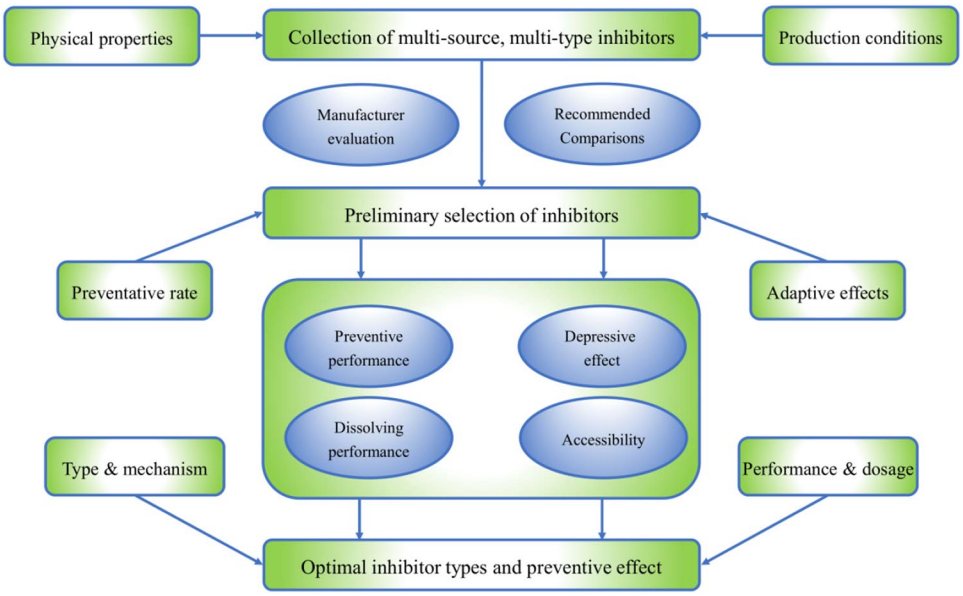

Fig. 4 The selection procedure of paraffin inhibitors

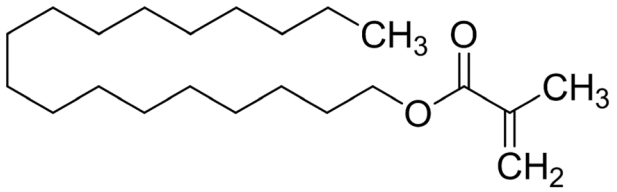

(a) Octadecyl methacrylate in BZ inhibitor

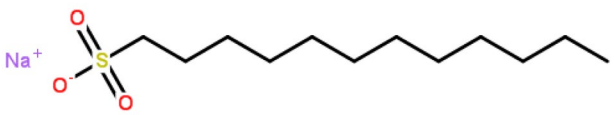

(b) Sodium dodecylbenzene sulfonate in PI inhibitor

Fig. 5 The main components of BZ and PI paraffin inhibitors

Phase change behavior

A thermodynamic model was selected to study the phase change process of gas-condensate wells, and the phase change behavior of three group condensate samples was calculated and determined. A gas–liquid–solid phase equilibrium equation and a modified PR equation are introduced (Daridon et al. 1993).

When the condensate is in gas–liquid–solid equilibrium, the temperature, pressure, and component fugacity of each phase are equal.

$$f_i^{\mathrm{V}}\left(T,P,x^{\mathrm{V}}\right)=f_i^{\mathrm{L}}\left(T,P,x^{\mathrm{L}}\right)=f_i^{\mathrm{S}}\left(T,P,x^{\mathrm{S}}\right) \tag{1}$$

$$f_i^{\mathrm{S}}=x_i^{\mathrm{S}}\gamma_i^{\mathrm{S}}f_i^{OS}\exp\left(\int_{P_0}^{P}\frac{\mathrm{V}_i^{\mathrm{S}}}{RT}\mathrm{d}P\right) \tag{2}$$

$$f_i^{\mathrm{L}}=x_i^{\mathrm{L}}\gamma_i^{\mathrm{L}}f_i^{OL}\exp\left(\int_{P_0}^{P}\frac{\mathrm{V}_i^{\mathrm{L}}}{RT}\mathrm{d}P\right) \tag{3}$$

$$\frac{x_i^{\mathrm{S}}}{x_i^{\mathrm{L}}}=K_i^{\mathrm{SL}}=\frac{\gamma_i^{\mathrm{L}}f_i^{OL}}{\gamma_i^{\mathrm{S}}f_i^{OS}} \tag{4}$$

where $f_i^{\mathrm{S}}\left(T,P,x^{\mathrm{S}}\right)$ is the fugacity of component i in the solid phase and is the same as f_i^{S}, $f_i^{\mathrm{L}}\left(T,P,x^{\mathrm{L}}\right)$ is the fugacity of component i in the liquid phase and is the same as f_i^{L}, γ_i^{S} is the activity coefficient of component i in solid phase, γ_i^{L} is the activity coefficient of component i in liquid phase, x_i^{S} is the molar fraction of component i in the solid phase, x_i^{L} is the molar fraction of component i in the liquid phase, $\exp\left(\int_{P_0}^{P}\frac{\mathrm{V}_i^{\mathrm{S}}}{RT}\mathrm{d}P\right)$ is the effect of pressure on solid phase, $\exp\left(\int_{P_0}^{P}\frac{\mathrm{V}_i^{\mathrm{L}}}{RT}\mathrm{d}P\right)$ is the effect of pressure on liquid phase, T is the system temperature K, P is the system pressure MPa, and P_0 is at atmospheric pressure 0.101325 MPa.

For gas and liquid phase fugacity, the calculation is based on the phase equilibrium equation for gas–liquid two-phase equilibrium state, while for solid phase fugacity under high-pressure condition, the calculation is as follows:

$$f_i^{\mathrm{V}}=\varphi_i^{\mathrm{V}}x_i^{\mathrm{V}}P \tag{5}$$

$$K_i^{\mathrm{VL}} = \frac{x_i^{\mathrm{V}}}{x_i^{\mathrm{L}}} = \frac{\varphi_i^{\mathrm{L}}}{\varphi_i^{\mathrm{V}}} \tag{6}$$

$$K^{\mathrm{SL}} = \frac{f_i^{\mathrm{S}}\varphi_i^{\mathrm{L}}P}{\gamma_i^{\mathrm{S}}f_i^{OS}\exp\left(\int_{P_0}^{P}\frac{\mathrm{V}_i^{\mathrm{S}}}{RT}\mathrm{d}P\right)f_i^{\mathrm{L}}} = \frac{\varphi_i^{\mathrm{L}}P}{\gamma_i^{\mathrm{S}}f_i^{OS}\exp\left(\int_{P_0}^{P}\frac{\mathrm{V}_i^{\mathrm{S}}}{RT}\mathrm{d}P\right)} \tag{7}$$

The gas–liquid–solid three-phase equilibrium is defined by the following equation.

$$\mathrm{V} + \mathrm{L} + \mathrm{S} = 1 \tag{8}$$

$$\mathrm{V}x_i^{\mathrm{V}} + \mathrm{L}x_i^{\mathrm{L}} + \mathrm{S}x_i^{\mathrm{S}} = z_i \tag{9}$$

$$\sum\nolimits_i x_i^{\mathrm{V}} = \sum\nolimits_i x_i^{\mathrm{L}} = \sum\nolimits_i x_i^{\mathrm{S}} = \sum\nolimits_i z_i = 1 \tag{10}$$

where V is the molar fraction of the gas phase, L is the liquid phase molar fraction, S is the molar fraction of solid phase, K_i^{SL} is the solid–liquid phase equilibrium constant of the component i, K_i^{VL} is the gas–liquid equilibrium constant of the component i, and z_i is the molar composition of component i.

$$\sum\nolimits_{i=1}^{n} x_i^{\mathrm{V}} = \sum\nolimits_{i=1}^{n} \frac{z_i K_i^{\mathrm{VL}}}{\mathrm{V}\left(K_i^{\mathrm{VL}} - 1\right) + \mathrm{S}\left(K_i^{\mathrm{SL}} - 1\right) + 1} = 1 \tag{11}$$

$$\sum\nolimits_{i=1}^{n} x_i^{\mathrm{L}} = \sum\nolimits_{i=1}^{n} \frac{z_i}{\mathrm{V}\left(K_i^{\mathrm{VL}} - 1\right) + \mathrm{S}\left(K_i^{\mathrm{SL}} - 1\right) + 1} = 1 \tag{12}$$

$$\sum\nolimits_{i=1}^{n} x_i^{\mathrm{S}} = \sum\nolimits_{i=1}^{n} \frac{z_i K_i^{\mathrm{SL}}}{\mathrm{V}\left(K_i^{\mathrm{VL}} - 1\right) + \mathrm{S}\left(K_i^{\mathrm{SL}} - 1\right) + 1} = 1 \tag{13}$$

The gravitational term coefficient a_λ and the bulk phase coefficient b_λ were modified to improve the prediction accuracy of the model for condensates, and to accurately describe the phase change characteristics of condensates, on the basis of Daridon modified equation and experimental results.

$$P = \frac{RT}{\mathrm{V} - b} - \frac{a\alpha(T)}{\mathrm{V}(\mathrm{V} + b) + b(\mathrm{V} - b)} \tag{14}$$

$$a = \lambda_a \frac{R^2 T_c^2}{P_c} \tag{15}$$

$$b = \lambda_b \frac{RT_c}{P_c} \tag{16}$$

The relationship between the gravitational correction factor and the volume correction factor is given by.

$$T_r < 1,\ \begin{cases} \lambda_a = 0.0513T_r^2 - 0.1325T_r + 0.5132 \\ \lambda_b = 0.0762T_r^2 - 0.0832T_r + 0.2342 \end{cases} \tag{17}$$

$$T_r \geq 1,\ \begin{cases} \lambda_a = -0.0621T_r^2 + 0.0756T_r + 0.4756 \\ \lambda_b = -0.0313T_r^2 + 0.0865T_r + 0.2652 \end{cases} \tag{18}$$

$$\omega = \frac{3}{7}\left[\frac{\left(T_b - 1\right)\log P_c}{T_c}\right] - 1 \tag{19}$$

$$\alpha(T) = \exp\left[m\left(1 - T_r\right)\right] \tag{20}$$

$$\begin{aligned} &\omega < 0.4,\ m = 0.418 + 1.58\omega - 0.580\omega^2 \\ &\omega \geq 0.4,\ m = 0.212 + 2.20\omega - 0.831\omega^2 \end{aligned} \tag{21}$$

where T is the system temperature K, P is the system pressure Pa, R is the ideal gas constant 8.3143 kJ/(kmol·K), $\alpha(T)$ is the temperature correlation for pure materials, V is the molar volume of the gas or liquid phase L/mol, a is the parameter, b is the parameter, T_c is the critical temperature K, P_c is the critical pressure Pa, T_r is the ratio of absolute to critical temperature, and ω is the acentric factor.

Results and discussion

Basic physical properties of condensate samples

The test results for appearance character, paraffin content, coarse crystalline paraffin content and it referred to C16 ~ C30, and paraffin appearance temperature are shown in Table 2, which shows that the average paraffin content of the collected condensate is 8.93%, and the average content

Table 2 Basic physical properties of condensate samples

Sample numbers	Appearance character	Paraffin content, %	C16 ~ C30 content, %	Paraffin appearance temperature, ℃
1#	Reddish brown translucent	8.10	13.62	9.30
2#	Reddish brown translucent	11.70	19.25	13.90
3#	Colorless transparence	7.00	8.15	12.60

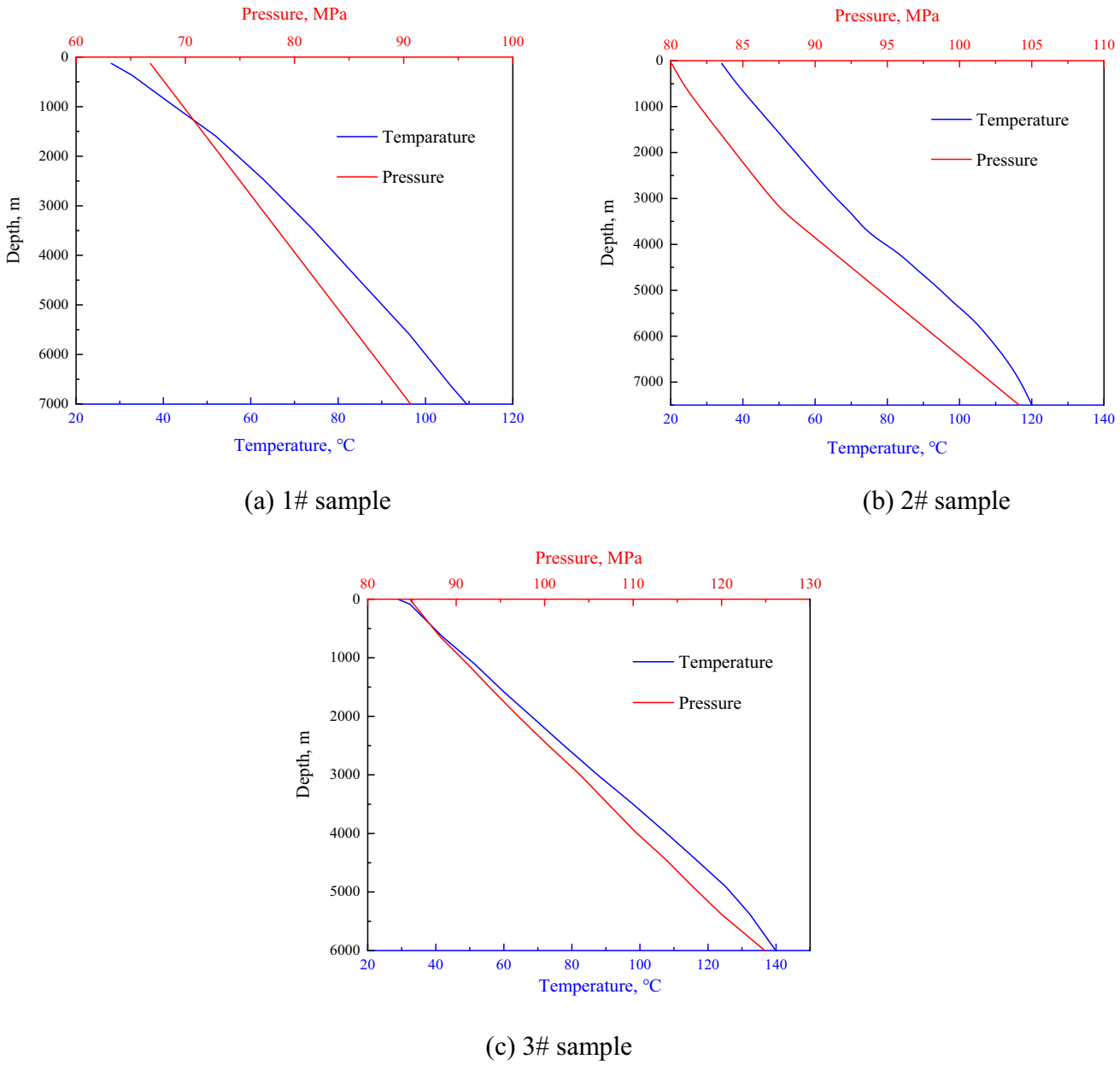

Fig. 6 Temperature and pressure profiles of three samples

of coarse crystalline paraffin is 13.67%. The paraffin content of condensate samples in this block is generally high, and there is a serious risk of paraffin deposition.

Temperature–pressure profile

As shown in Fig. 6, the temperature gradually decreases during the production of gas-condensate wells, and the overall trend of the temperature profile slope becomes larger, which indicates that an increasing temperature drop, and the single well in the block shows similar characteristics of the temperature profile. The pressure decreases gradually, and the slope of the pressure profile does not show a significant trend, which indicates that a constant pressure drop along well depth, and the single well in the block shows similar pressure distribution characteristics.

For pressure drop losses along the well depth for three groups, which are similar for three groups are around 25 MPa. For temperature, their average temperature drop is approximately 80 ℃. However, 2# sample shows a

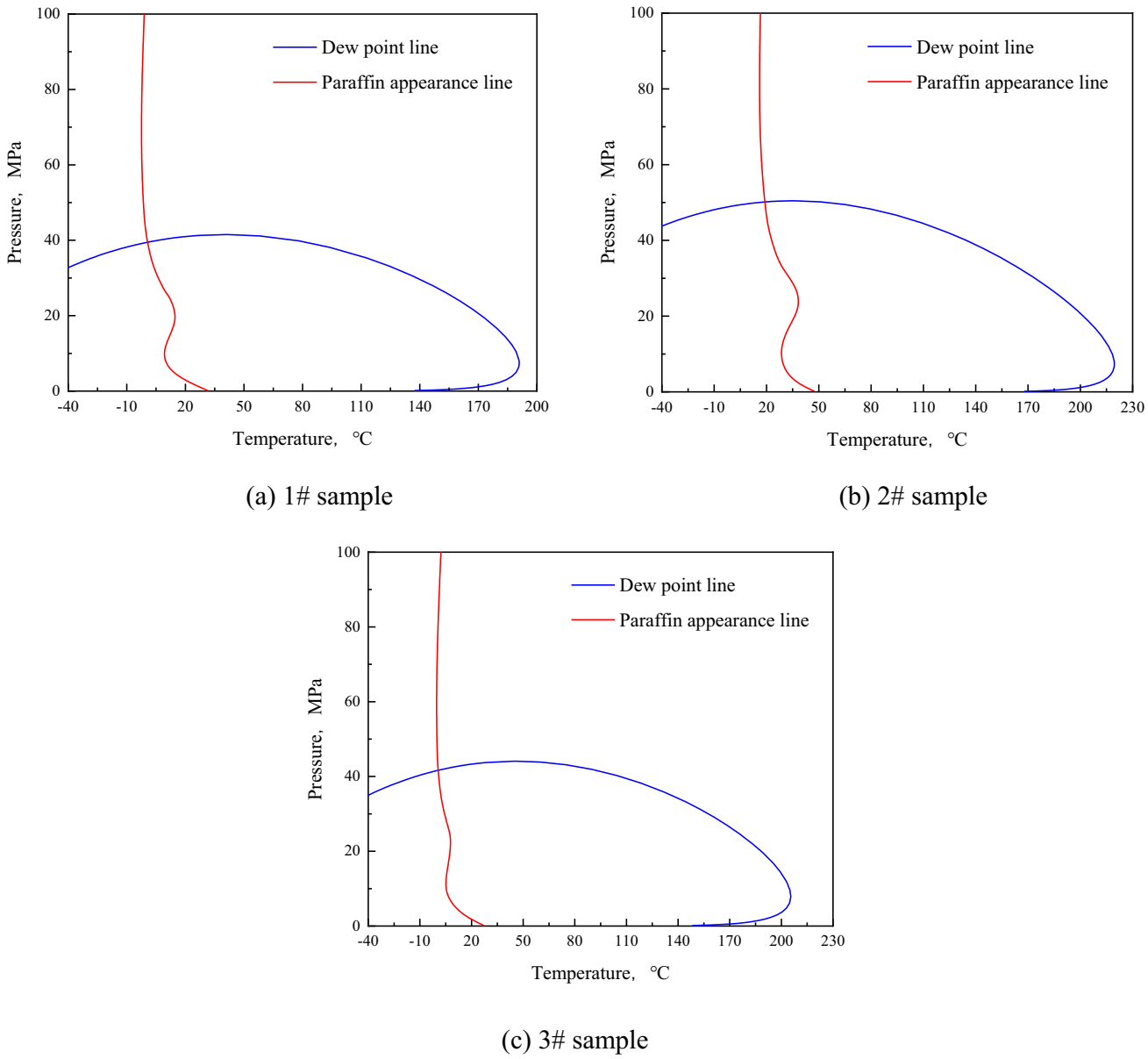

Fig. 7 Phase change diagram of three samples

relatively flat and slightly turning change compared to the other two samples.

Phase change behavior

As shown in Fig. 7, the dew point pressures of three samples were 39.70, 37.40 and 45.40 MPa, respectively, while the wellhead temperatures of 2# sample were higher than the calculated paraffin appearance temperature. This indicates that the oil temperature-driven paraffin deposition process does not occur in the gas-condensate wellbore. The temperature and pressure distributions in the wellhead area are only for the gas–liquid phase equilibrium transition, whereas the temperature and pressure distributions in the wellbore are essentially for the gas phase (Guo et al. 2020; Kutcherov and Lopatin 2019; Ferreira et al. 2018).

The temperature–pressure profile (Fig. 6) shows that the dew point pressure decreases with temperature increase, mainly occurring in the wellbore, where the solubility of the heavy components in the gas phase decreases under lower temperatures and higher dew point pressures conditions. So that they deposit more easily to form droplets. The paraffin appearance line reflects that the paraffin appearance temperature is less influenced by pressure and fluctuates more significantly below its intersection with the dew point line, which is increasing and then decreasing as the pressure

(a) Initial stage (b) Middle stage (c) End stage

Fig. 8 Different stages of paraffin deposition in the experiment

decreases. This indicates that due to the oil pressure below the pressure of intersections, the heavier components deposit preferentially to form droplets, where the paraffin deposition at a high temperature, followed by a low carbon number distribution of paraffin component.

The identification chart of paraffin deposition

As shown in Fig. 8, the paraffin deposition behavior at different stages during the cold plate deposition experiment. The deposition critical boundary of gas-condensate wells was identified and the deposition critical boundary diagram was constructed, by the paraffin deposition experiments.

The temperature and pressure profiles are combined to identify the paraffin deposition location in the identification graphic, and the deposition rate can also be determined, as shown in Fig. 9.

The left plot represents the paraffin deposition rate identification graphic under the corresponding position, while the right plot represents the regions of paraffin deposition in the wellbore, as shown in Fig. 9a, b, and c. The red dashed area in the right subplot of Fig. 9 represents the deposition thickness of the horizontal cross section of paraffin deposition as determined experimentally within the upper 2500 m region of gas-condensate wells. It indicates the deposition thickness growth rate corresponding to that depth. The blue line in the left subplot represents the boundary of the set of temperature–pressure points corresponding to a certain depositional rate. It can subsequently be used to find the corresponding deposition growth rate on the left subplot based on the relationship between temperature, pressure, and depth of each well. According to the temperature–pressure profile of the wellbore, the corresponding well depth location was identified by the correspondence paraffin deposition rate and temperature–pressure distribution. As shown in Fig. 9a, the maximum deposition rate of 1# sample is 15.50 mm/year, and the corresponding temperature and pressure are 45 ℃ and 70 MPa, which identifies its centralized deposition boundary within 1000 ~ 1500 m. As shown in Fig. 9b, the maximum deposition rate of 2# sample is 10.79 mm/year, with the corresponding temperature and pressure of 50 ℃ and 84 MPa, which identifies its centralized deposition location in 1500 ~ 2000 m. As shown in Fig. 9c, the maximum deposition rate of 3# sample is at 14.98 mm/year, corresponding to a temperature and pressure of 45 ℃ and 88 MPa, identifying its concentrated deposition location in the 1000 ~ 1500 m.

Preventive effect of two types of paraffin inhibitors

Paraffin's deposition prevention properties

The paraffin preventive rates of two types of paraffin inhibitors collected by the crude oil dynamic paraffin deposition rate tester. The prevention effect of paraffin inhibitors was compared at 1.00 wt.% concentration, and the paraffin prevention rate was taken as the judgment index. Two types of inhibitors with better performance were selected, namely BZ and PI, as shown in Fig. 10. BZ inhibitor is a paraffin inhibitor (paraffin crystal modifier), and PI inhibitor is a paraffin dispersant. The paraffin preventive rates of both BZ and PI were similarly above 90%, with an average of 95.04 and 94.67%.

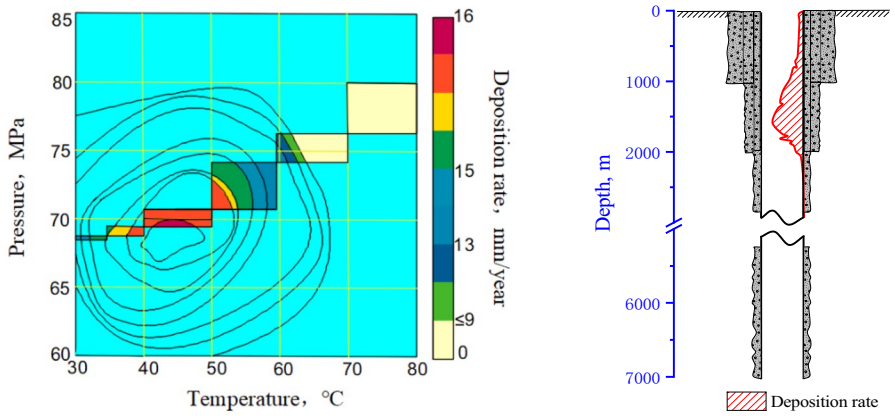

(a) 1# sample

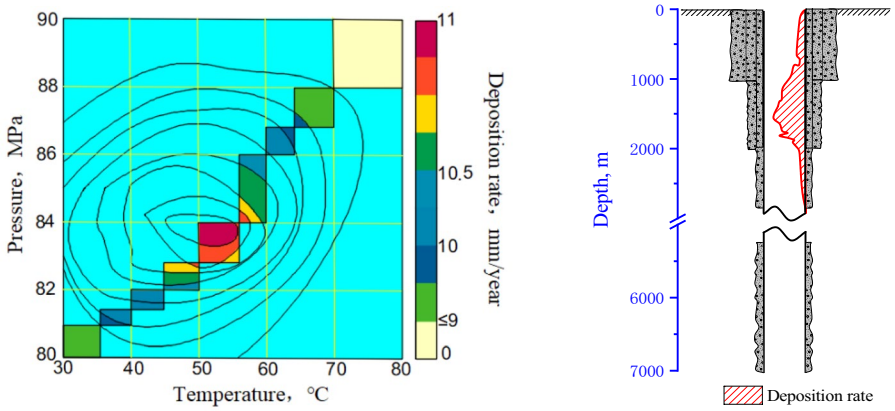

(b) 2# sample

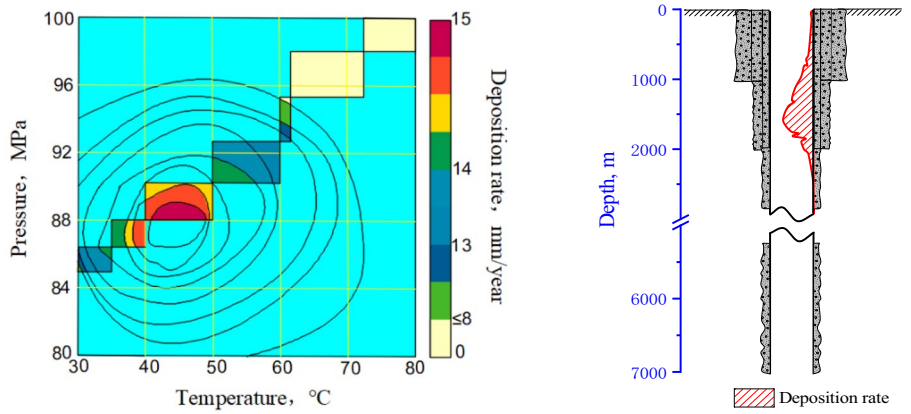

(c) 3# sample

Fig. 9 The identification graphic of paraffin deposition

The performance of reducing paraffin appearance temperature

The performance of reducing the paraffin appearance temperature of two types of paraffin inhibitors collected by the DSC experiment apparatus. The effect on the characteristic temperature distribution of paraffin appearance for condensate samples at 1.00 wt.% concentration is shown in Fig. 11. The common paraffin inhibitors available could reduce the paraffin appearance temperature of condensate samples

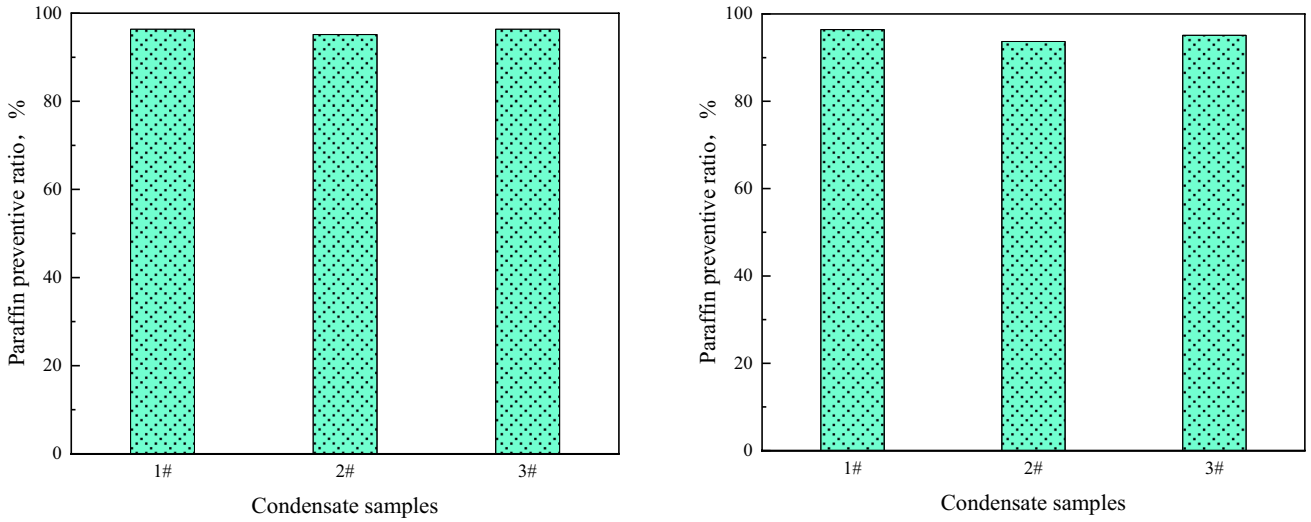

Fig. 10 Paraffin preventive rate of two types of inhibitors

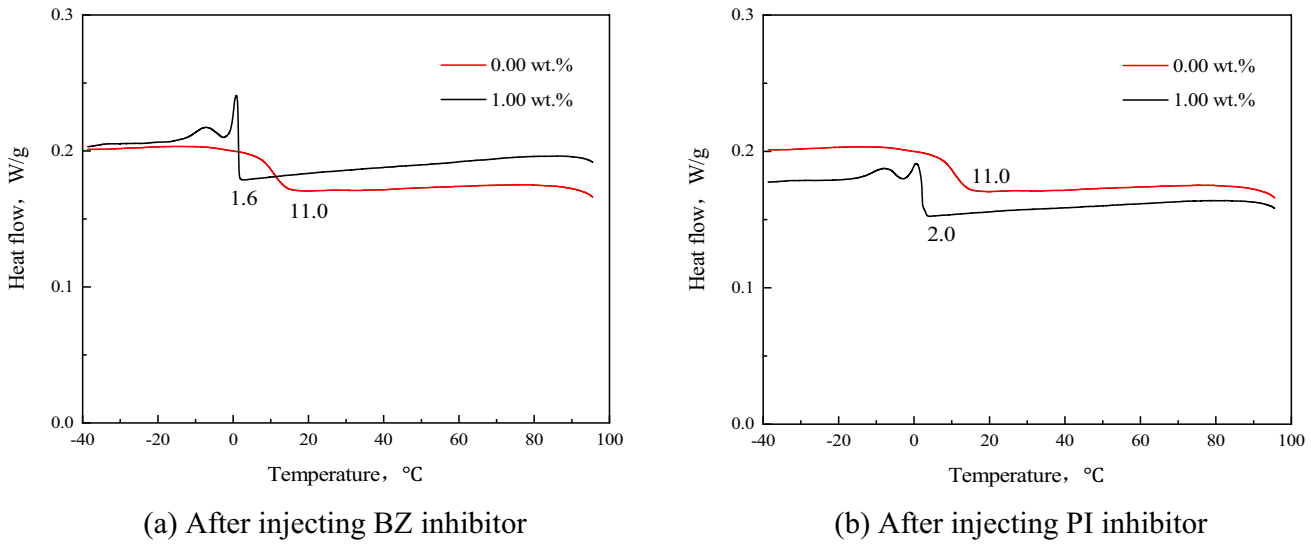

Fig. 11 The performance of reducing the paraffin appearance temperature of two types of inhibitors

Table 3 Experimental results on dissolving paraffin properties of paraffin inhibitors

Inhibitor	Dissolving paraffin rate of sliced paraffin, g/min	Dissolving paraffin rate of collected paraffin, g/min	Technical standard, g/min
BZ	0.0170	0.0163	≥0.0160
PI	0.0191	0.0169	

more than half. However, the two types of paraffin inhibitors selected for the experiments can reduce the paraffin appearance temperature approximately 10 ℃, and the reduction can reach more than 80%.

Dissolving paraffin properties

The evaluation results of dissolving paraffin performance for sliced paraffin and actual collected paraffin from gas-condensate wells are shown in Table 3. It can be seen that PI paraffin inhibitor has the best dissolving paraffin performance, and their dissolving rate can reach 0.0191 and 0.0169 g/min, respectively. They both fulfill the technical

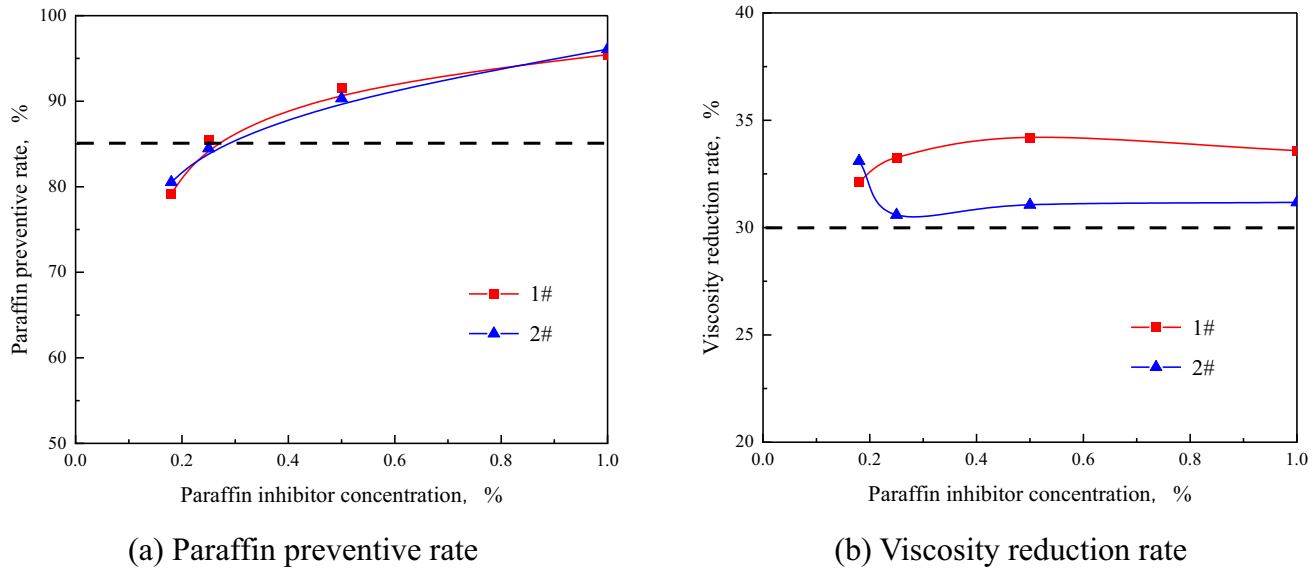

(a) Paraffin preventive rate (b) Viscosity reduction rate

Fig. 12 Effect of dosage on paraffin preventive rate and viscosity reduction rate for BZ inhibitor

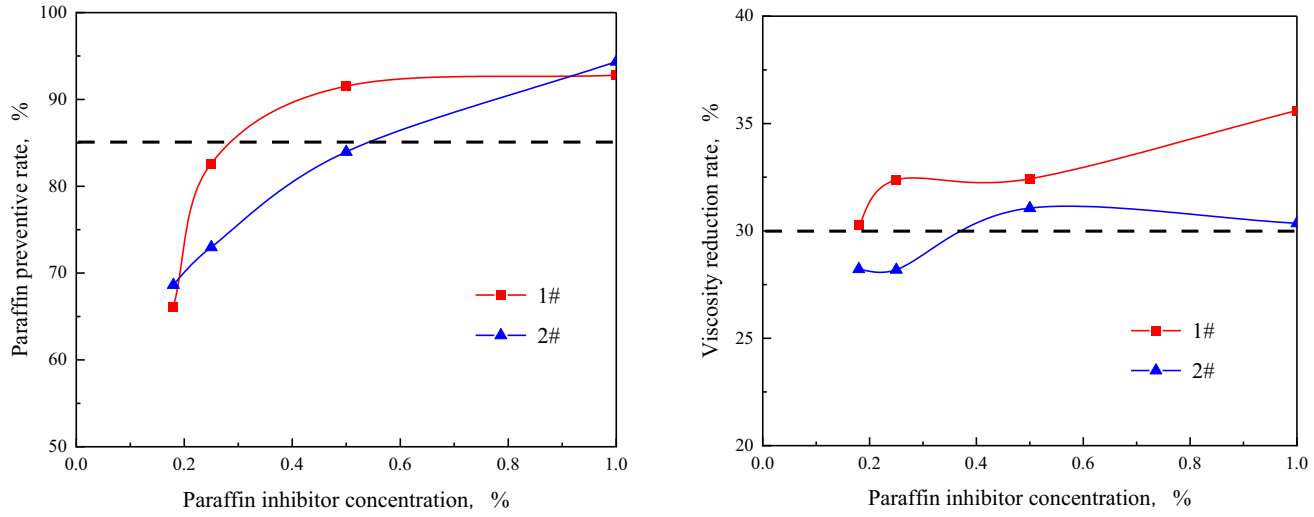

(a) Paraffin preventive rate (b) Viscosity reduction rate

Fig. 13 Effect of dosage on paraffin preventive rate and viscosity reduction rate for PI inhibitor

standard that dissolving paraffin rate is more than 0.0160 g/min.

Effect of dosage on preventive properties

The paraffin preventive rates and the viscosity reduction rate of two types of paraffin inhibitors collected by the crude oil dynamic paraffin deposition rate tester. The experimental results of the paraffin prevention rate and viscosity reduction rate of condensate samples at 1.00, 0.50, 0.25 and 0.18 wt.% concentrations for BZ and PI paraffin inhibitors are shown in Figs. 12 and 13.

The dashed lines in Figs. 12 and 13 indicate the average paraffin preventive and viscosity reduction rates of the two types of paraffin inhibitors, BZ and PI, in the experiments, which were around 85 and 30%, respectively. The dashed line is embedded into the graph to reflect the difference between the paraffin preventive rate and viscosity reduction rate and the average value at different concentrations to achieve the comparative effect. It can be seen that for BZ paraffin inhibitor, the viscosity reduction rate of

condensate samples at different concentrations is concentrated in 30 ~ 35%. When the concentration is above 0.50 wt.%, the paraffin preventive rate is above 90%. When the concentration is decreased to 0.25 wt.%, the paraffin preventive rate is approximately 85%, and when the concentration is further decreased to 0.18 wt.%, the paraffin prevention rate will even be below 80%.

For the PI paraffin inhibitor, when the concentration was decreased from 1.00 to 0.50 wt.%, the paraffin preventive rate remained above 90% for the 1# sample, but decreased to below 85% for the 2# sample. When the concentration was decreased to 0.25 wt.%, the paraffin preventive rate was 82.61 and 72.97% for 1# and 2# samples, respectively. When the concentration was dropped to 0.18 wt.%, the paraffin preventive rate decreased to less than 70%. The viscosity reduction rate of 1# sample could get more than 30% under different concentrations, but the viscosity reduction rate of 2# sample was less than 30% when the concentration was below 0.50 wt.%.

Effect of dosage on paraffin appearance temperature

The performance of reducing the paraffin appearance temperature of two types of paraffin inhibitors collected by the DSC experiment apparatus. The characteristic temperature changes of paraffin appearance of after injecting 1.00, 0.50 and 0.25 wt.% concentrations of BZ and PI paraffin inhibitors are shown in Fig. 14.

It can be seen that the paraffin appearance temperature decreases to different degrees with increasing dosages of paraffin inhibitors. For the collected condensate samples, the difference in paraffin appearance temperature between the three dosages of PI paraffin inhibitor was 1–2 ℃. In contrast, the paraffin appearance temperature of BZ paraffin inhibitor at 0.25 wt.% was 2–3 ℃, which is higher than that of 1.00 and 0.50 wt.%. This shows a 54.6% reduction in paraffin appearance temperature.

Further comparative analysis suggests that the optimal concentration of BZ paraffin inhibitor is 0.25–0.50 wt.%, and the optimal concentration of PI paraffin inhibitor is 0.50–1.00 wt.%.

Effect of paraffin inhibitors on the microstructure of paraffin crystals

The results of effect of paraffin inhibitors on the microstructure of paraffin crystals are gained by the polarizing microscope. The effect of BZ and PI paraffin inhibitors on the microstructure of paraffin crystals at 0.50 wt.% concentration is shown in Fig. 15. The two paraffin inhibitors at a dosage of 0.50 wt.% showed a change in the morphology of the paraffin crystals, when appeared at temperatures lower than 5 ℃. Compared to before injecting the agent, with vague, blurred morphology in the visual field, no distinctive angles, and their crystalline bonding visible.

The paraffin crystal modifier includes non-polar parts of the main and branched chains that can be eutectic with paraffin molecules, and polar parts that distort the shape of paraffin crystals, as shown in Fig. 16. The paraffin crystals are in a dispersed state when the temperature of the paraffin crystals is above the paraffin appearance temperature. The growth and agglomeration of the paraffin crystals occur when the temperature is below the paraffin appearance temperature,

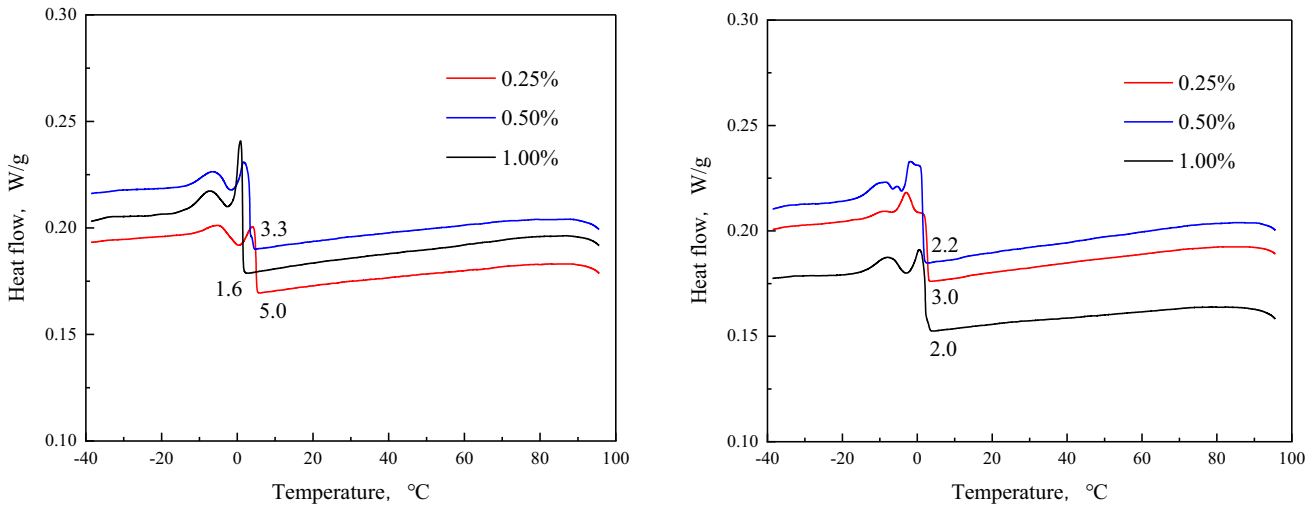

(a) Injecting BZ paraffin inhibitors

(b) Injecting PI paraffin inhibitors

Fig. 14 Effect of inhibitors dosage on paraffin appearance temperature

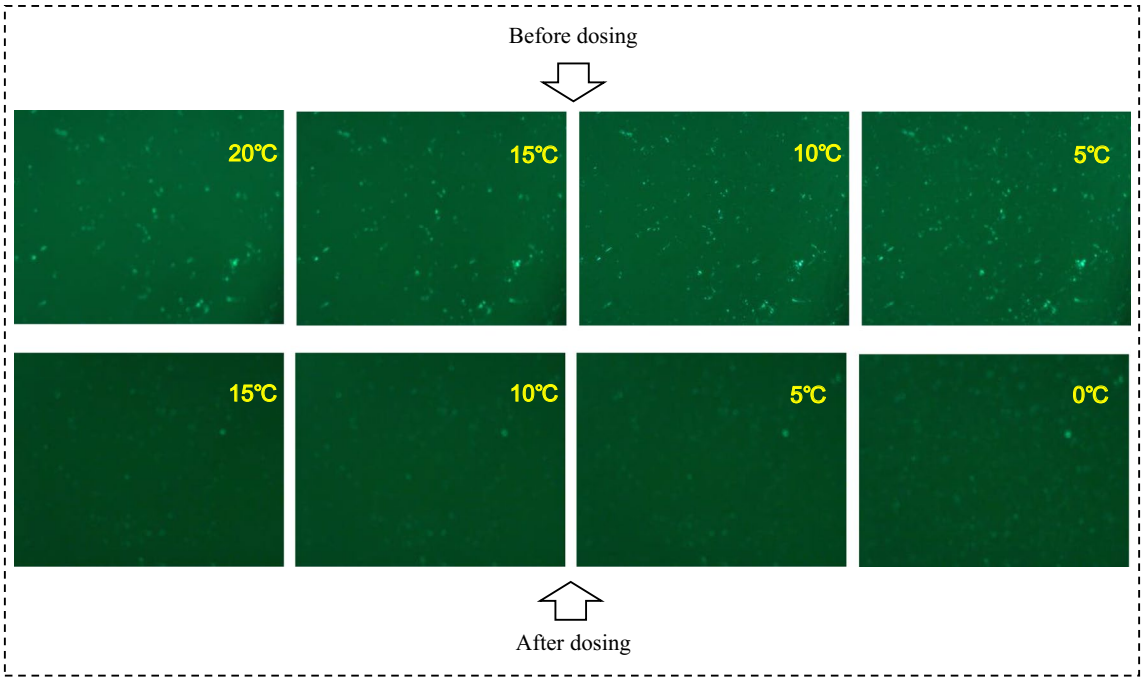

(a) Before and after injecting BZ paraffin inhibitor

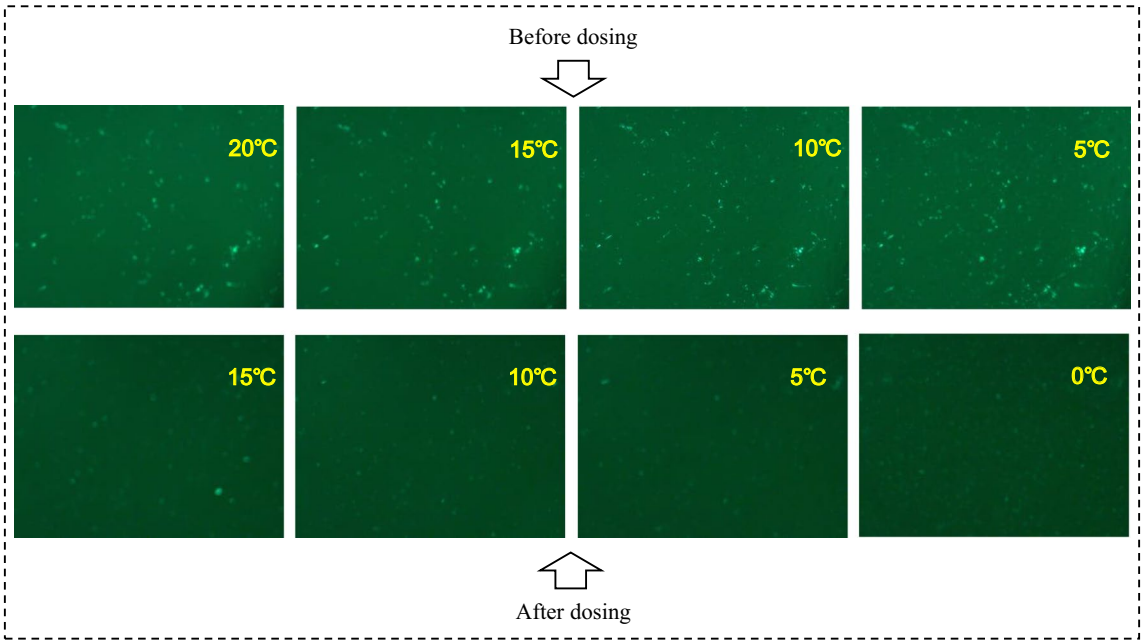

(b) Before and after injecting PI paraffin inhibitor

Fig. 15 Effect of paraffin inhibitors on the microstructure of paraffin crystals

and the paraffin crystals will finally deposit on the cold surface. Once the paraffin crystal modifier is incorporated into the system, the crystal modifier (CM) will aggregate and cross-link with the paraffin crystals and could further strip the paraffin crystals adhering to the cold surface and hinder the paraffin deposition. They change the morphology of the paraffin crystals and the spatial network structure and inhibit paraffin deposition. A network structure could be formed throughout the oil phase, so that the formed crystals are

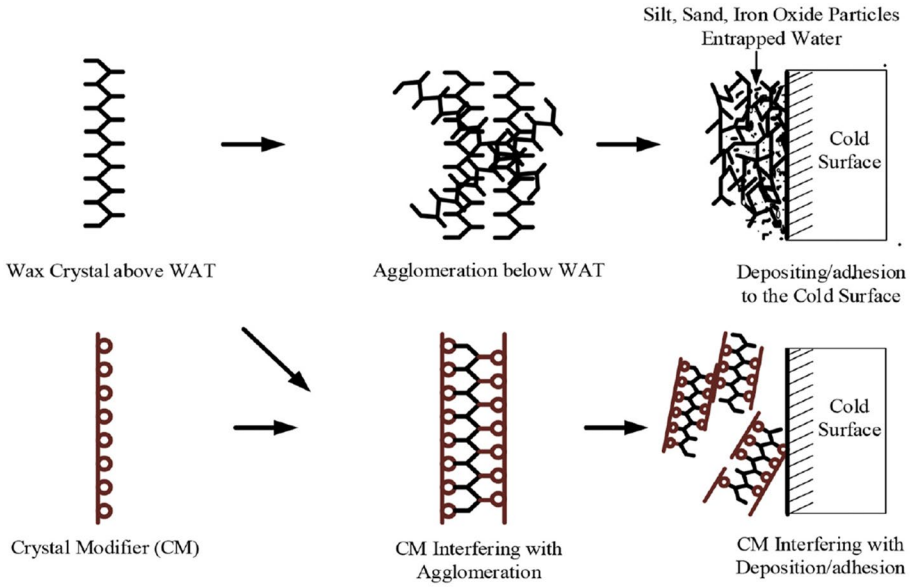

Fig. 16 Interaction mechanisms between paraffin crystals modifier with paraffin crystals (Sousa et al. 2019)

dispersed and unable to aggregate (Lashkarbolooki et al. 2011; Elganidi et al. 2020).

Conclusions

The current study is concentrated on the treatment on paraffin deposition behavior in gas-condensate wells with chemical inhibitors. The cold plate structure was designed to increase the deposition area to easily observe the deposition on the surface of the cold finger. The experimentally obtained diagrams can facilitate the determination of the paraffin deposition boundary in the wellbore and quantitatively characterize the rate of paraffin deposition. And the optimal concentration of two types of paraffin inhibitors, BZ and PI, was determined by experiment. The obtained results can be classified as below.

1. The temperature and pressure decreased gradually during the lifting process, and the slope of the temperature distribution profile was larger, and the pressure distribution varied significantly under the conditions of similar well depth and wellhead temperature, which was influenced by the production rate and oil–gas ratio. The phase change behavior, combined with the temperature–pressure profile, reflects the predominance of gas phase within gas-condensate wells.
2. The paraffin deposition critical boundary for gas-condensate wells under universal wellhead temperature conditions was within the range of 1000 ~ 1500 m, which the cold plate deposition experiments. The maximum deposition rate was 15.50 mm/year, which matched the temperature and pressure conditions of 45 ℃ and 70 MPa. And the establishment of a graphic that can identify the deposition rate at different depth conditions of the gas-condensate well, quantitative prediction in the field can be achieved.
3. Paraffin crystal modifier is more suitable for gas-condensate wells, the optimal concentration is 0.25 ~ 0.50 wt.%, and the paraffin prevention rate can reach 85 ~ 95%. It can decrease the paraffin appearance temperature approximately 40% and significantly modify paraffin crystal morphology, which could achieve long-term prevention.

Funding This work presented in this paper was financially supported by the National Natural Science Foundation of China (Grant No. 52174060; 52074090).

Declarations

Conflict of interest The authors declare no conflict of interest.

References

Anisuzzaman SM, Abang S, Bono A et al (2017) Wax inhibitor based on ethylene vinyl acetate with methyl methacrylate and diethanolamine for crude oil pipeline. IOP Conf Ser: Mater Sci Eng 206:012074. https://doi.org/10.1088/1757-899X/206/1/012074

Azevedo LFA, Teixeira AM (2003) A critical review of the modeling of wax deposition mechanisms. Pet Sci Technol 21(3–4):393–408. https://doi.org/10.1081/LFT-120018528

Behesht Abad AR, Mousavi S, Mohamadian N et al (2021) Hybrid machine learning algorithms to predict condensate viscosity in the near wellbore regions of gas condensate reservoirs. J Nat Gas Sci Eng 95:104210. https://doi.org/10.1016/j.jngse.2021.104210

Chi Y, Daraboina N, Sarica C (2017) Effect of the flow field on the wax deposition and performance of wax inhibitors: cold finger and flow loop testing. Energy Fuels 31(5):4915–4924. https://doi.org/10.1021/acs.energyfuels.7b00253

Danilović DS, Karović Maričić VD, Čokorilo VB (2010) Solving paraffin deposition problem in tubing by heating cable application. Therm Sci 14(1):247–253. https://doi.org/10.2298/TSCI1001247D

Daridon JL, Lagourette B, Saint-Guirons H, Xans P (1993) Cubic equation of state model for phase equilibrium calculation of alkane+carbon dioxide+water using a group contribution kij. Fluid Phase Equilib 91(1):31–54. https://doi.org/10.1016/0378-3812(93)85077-Y

Elarbe B, Elganidi I, Ridzuan N et al (2022) Synthesis, characterization and evaluation of stearyl acrylate-co-behenyl acrylat e copolymer as a pour point depressant of waxy crude oil. J Pet Explor Prod Technol 12(7):1811–1828. https://doi.org/10.1007/s13202-021-01408-7

Elganidi I, Elarbe B, Abdullah N, Ridzuan N (2020) Synthesis of a novel terpolymer of (BA-co-SMA-co-MA) as pour point depressants to improve the flowability of the Malaysian crude oil. Mater Today Proc 42:28–32. https://doi.org/10.1016/j.matpr.2020.08.628

Elganidi I, Elarbe B, Ridzuan N, Abdullah N (2022) Synthesis, characterisation and pre-evaluation of a novel terpolymer as pour point depressants to improve the Malaysian crude oil flowability. J Pet Explor Prod Technol 12(7):2067–2081. https://doi.org/10.1007/s13202-021-01445-2

Elkatory MR, Hassaan MA, Soliman EA et al (2023) Influence of poly (benzyl oleate-co-maleic anhydride) pour point depressant with Di-Stearyl amine on waxy crude oil. Polymers 15(2):306. https://doi.org/10.3390/polym15020306

Faraji F, Ugwu JO, Chong PL, Nabhani F (2020) Modelling viscosity of liquid dropout near wellbore region in gas condensate reservoirs using modern numerical approaches. J Pet Sci Eng 185:106604. https://doi.org/10.1016/j.petrol.2019.106604

Ferreira FAV, Barbalho TCS, Araújo IRS, Oliveira HNM, Chiavone-Filho O (2018) Characterization, pressure-volume-temperature properties, and phase behavior of a condensate gas and crude oil. Energy Fuels 32(4):5643–5649. https://doi.org/10.1021/acs.energyfuels.8b00469

Gan Y, Cheng Q, Wang Z et al (2019) Molecular dynamics simulation of the microscopic mechanisms of the dissolution, diffusion and aggregation processes for waxy crystals in crude oil mixtures. J Pet Sci Eng 179:56–69. https://doi.org/10.1016/j.petrol.2019.04.059

Ghiasi MM, Shahdi A, Barati P, Arabloo M (2014) Robust modeling approach for estimation of compressibility factor in retrograde gas condensate systems. Ind Eng Chem Res 53:12872–12887. https://doi.org/10.1021/ie404269b

Guo P, Liu H, Wang C et al (2020) The determination of phase behavior properties of high-temperature high-pressure and rich condensate gases. Fuel 280:118568. https://doi.org/10.1016/j.fuel.2020.118568

Han J, Wu G, Yang H et al (2021) Type and genesis of condensate gas reservoir in the Tazhong uplift of the Tarim Basin. Nat Gas Ind 41(7):24–32. https://doi.org/10.3787/j.issn.1000-0976.2021.07.003

Hassan A, Mahmoud M, Al-Majed A et al (2019) Gas condensate treatment: a critical review of materials, methods, field applications, and new solutions. J Pet Sci Eng 177:602–613. https://doi.org/10.1016/j.petrol.2019.02.089

Hernandez OC, Hensley HD, Sarica C et al (2004) Improvements in single-phase paraffin deposition modeling. SPE Prod Facil 19(4):237–244. https://doi.org/10.2118/84502-PA

Hoffmann R, Amundsen L (2009) Single-phase wax deposition experiments. Energy Fuels 24(2):1069–1080. https://doi.org/10.1021/ef900920x

Hong J, Wang Z, Li J et al (2023) Effect of interface structure and behavior on the fluid flow characteristics and phase interaction in the petroleum industry: State of the art review and outlook. Energy Fuels 37(14):9914–9937. https://doi.org/10.1021/acs.energyfuels.3c00809

Huang Z, Lee HS, Senra M, Scott Fogler H (2011) A fundamental model of wax deposition in subsea oil pipelines. AIChE J 57(11):2955–2964. https://doi.org/10.1002/aic.12517

Ibrahim HEH, Gad A, EL-Kasaby M, Ebrahim S, Kandil S, (2023) Study on the influence of poly (m-aminophenol) as pour point depressant of paraffinic crude oil. Pet Sci Technol 41(1):1–13. https://doi.org/10.1080/10916466.2021.1992423

Kurniawan M, Ruwoldt J, Norrman J, Paso KG (2021) Influence of wax inhibitor molecular weight on solution crystallization and rheology of monodisperse waxes. Energy Fuels 35(9):7666–7680. https://doi.org/10.1021/acs.energyfuels.0c04187

Kutcherov VG, Lopatin AS (2019) Properties and phase behavior of Shtokman gas condensate at high pressure. Pet Sci Technol 37(9):1099–1105. https://doi.org/10.1080/10916466.2019.1575876

Lashkarbolooki M, Esmaeilzadeh F, Mowla D (2011) Mitigation of wax deposition by wax-crystal modifier for Kermanshah crude oil. J Dispers Sci Technol 32(7):975–985. https://doi.org/10.1080/01932691.2010.488514

Lekomtsev A, Kozlov A, Kang W, Dengaev A (2022) Designing of a washing composition model to conduct the hot flushing wells producing paraffin crude oil. J Pet Sci Eng 217:110923. https://doi.org/10.1016/j.petrol.2022.110923

Ma Q, Wang W, Liu Y et al (2017) Wax adsorption at paraffin oil-water interface stabilized by Span80. Colloid Surf A 518:73–79. https://doi.org/10.1016/j.colsurfa.2017.01.023

Mahir LHA, Vilas Bôas Fávero C, Ketjuntiwa T, Fogler HS, Larson RG (2019) Mechanism of wax deposition on cold surfaces: gelation and deposit aging. Energy Fuels 33(5):3776–3786. https://doi.org/10.1021/acs.energyfuels.8b03139

Makwashi N, Zhao D, Abdulkadir M, Ahmed T, Muhammad I (2021) Study on waxy crudes characterisation and chemical inhibitor assessment. J Pet Sci Eng 204:108734. https://doi.org/10.1016/j.petrol.2021.108734

Ochieng FO, Kinyanjui MN, Abonyo JO, Kiogora PR et al (2022) Mathematical modeling of wax deposition in field-scale crude oil pipeline systems. J Appl Math 2022:2845221. https://doi.org/10.1155/2022/2845221

Ragunathan T, Husin H, Wood CD (2020) Wax formation mechanisms, wax chemical inhibitors and factors affecting chemical inhibition. Appl Sci 10(2):479. https://doi.org/10.3390/app10020479

Ragunathan T, Wood CD, Husin H (2022a) The influence of palm oil additives on the pour point and wax deposition tendencies of Chenor crude oil. J Pet Explor Prod Te 12(3):589–599. https://doi.org/10.1007/s13202-021-01316-w

Ragunathan T, Wood CD, Husin H (2022b) Inhibiting wax deposition using palm oil additives. J Pet Explor Prod Te 12(1):99–115. https://doi.org/10.1007/s13202-021-01318-8

Shi B, Wang Z, Zhang Z, Xu Y, Ling K (2022) A state of the art review on the wellbore blockage of condensate gas wells: towards understanding the blockage type, mechanism, and treatment. Lithosphere 12:2–18. https://doi.org/10.2113/2022/8076631

Singh P, Venkatesan R, Fogler HS, Nagarajan N (2000) Formation and aging of incipient thin film wax-oil gels. AIChE J 46(5):1059–1074. https://doi.org/10.1002/aic.690460517

Sousa AL, Matos HA, Guerreiro LP (2019) Preventing and removing wax deposition inside vertical wells: a review. J Pet Explor Prod Technol 9(3):2091–2107. https://doi.org/10.1007/s13202-019-0609-x

Sousa AM, Matos HA, Guerreiro L (2020) Wax deposition mechanisms and the effect of emulsions and carbon dioxide injection on wax deposition: critical review. Petroleum 6(3):215–225. https://doi.org/10.1016/j.petlm.2019.09.004

Subramanie P, Vijayakumar SD, Ridzuan N (2021) Effect of wax inhibitor and sodium cloisite, Na+ nanoparticle on wax deposition of Malaysian crude oil through cold finger analysis. Pet Sci Technol 39(19–20):860–877. https://doi.org/10.1080/10916466.2021.1973496

Szuflita S, Pajda M, Kuśnierczyk J, Wojnicki M, Marcin W (2020) Studies on the efficiency of the impact of paraffin inhibitors on lowering the WAT temperature and reducing the amount of paraffin deposit. Energies 13(18):4653. https://doi.org/10.3390/en13184653

Van Der Geest C, Guersoni VCB, Merino-Garcia D, Bannwart AC (2018) Wax deposition experiment with highly paraffinic crude oil in laminar single-phase flow unpredictable by molecular diffusion mechanism. Energy Fuels 32(3):3406–3419. https://doi.org/10.1021/acs.energyfuels.8b00269

Van Der Geest C, Melchuna A, Bizarre L, Bannwart AC, Guersoni VCB (2021) Critical review on wax deposition in single-phase flow. Fuel 293:120358. https://doi.org/10.1016/j.fuel.2021.120358

Wang Z, Xu Y, Zhao Y et al (2019) Role of shearing dispersion and stripping in wax deposition in crude oil pipelines. Energies 12(22):4325. https://doi.org/10.3390/en12224325

Wang Z, Wang H, Zhu C, Rui Z, Liu Y (2020) A novel method for characterizing the aggregation of wax crystals and an improvement in wax deposition modeling. J Energ Resour 142(10):103003. https://doi.org/10.1115/1.4047083

Wang Z, Liu X, Li J et al (2022a) Effect of a coated wall on wax-asphaltene molecule diffusion, aggregation, and adhesion mechanism: a molecular dynamics simulation study. Energy Fuels 36(17):10191–10204. https://doi.org/10.1021/acs.energyfuels.2c02183

Wang Z, Liu X, Zhang H et al (2022b) Modeling of kinetic characteristics of alkaline-surfactant-polymer-strengthened foams decay under ultrasonic standing wave. Pet Sci 19(4):1825–1839. https://doi.org/10.1016/j.petsci.2022.04.012

Wang W, Wu K, Chen Z et al (2022c) Non-equilibrium pressure drop method for alleviating retrograde condensate effect on gas condensate well deliverability. Acta Pet Sin 43(5):719–726. https://doi.org/10.7623/syxb202205012

Wang Z, Xu Y, Gan Y et al (2022d) Micromechanism of partially hydrolyzed polyacrylamide molecule agglomeration morphology and its impact on the stability of crude oil-water interfacial film. J Pet Sci Eng 214:110492. https://doi.org/10.1016/j.petrol.2022.110492

Wang Z, Xu Y, Khan N, Zhu C, Gao Y (2023) Effects of the surfactant, Polymer, and crude oil properties on the formation and stabilization of oil-based foam liquid films: Insights from the microscale. J Mol Liq 373:121194. https://doi.org/10.1016/j.molliq.2022.121194

Xu Y, Wang H, Wang Z et al (2021) Microscopic mechanism of asphaltene and resin behavior to the stability of oil-water interface. J Northeast Pet Univ 45(6):90–101. https://doi.org/10.3969/j.issn.2095-4107.2021.06.008

Yaghy G, Ali A, Charpentier TVJ et al (2021) Wax deposition using a cold rotating finger: an empirical and theoretical assessment in thermally driven and sloughing regimes. J Pet Sci Eng 200:108252. https://doi.org/10.1016/j.petrol.2020.108252

Zhang J, Wu C, Li W, Wang Y, Han Z (2003) Study on performance mechanism of pour point depressants with differential scanning calorimeter and X-ray diffraction methods. Fuel 82(11):1419–1426. https://doi.org/10.1016/S0016-2361(03)00028-0

Zhao J, Xi X, Dong H, Wang Z, Zhuo Z (2022) Rheo-microscopy in situ synchronous measurement of shearing thinning behaviors of waxy crude oil. Fuel 323:124427. https://doi.org/10.1016/j.fuel.2022.124427

Zhong H, He Y, Yang E, Bi Y, Yang T (2022) Modeling of microflow during viscoelastic polymer flooding in heterogenous reservoirs of Daqing oilfield. J Pet Sci Eng 210:110091. https://doi.org/10.1016/j.petrol.2021.110091